Adsorption (2007) 13: 267–279
DOI 10.1007/s10450-007-9019-3

Novel zeolite composites and consequences for rapid sorption processes

Alfons Brandt · Martin Bülow · Anna Deryło-Marczewska · Jacek Goworek · Jens Schmeißer · Wolfgang Schöps · Baldur Unger

Received: 25 April 2007 / Revised: 30 June 2007 / Accepted: 11 July 2007 / Published online: 14 September 2007

Abstract Novel sorbents for rapid dynamic sorption processes based on the concept of sorption-active shell/sorption-inert core composite granules are presented. Tailoring such composites to a technical sorption process is exemplified by NaX and LiLSX zeolites as sorption-active components. Composite granules are characterized by various techniques specifically by oxygen-VPSA pilot-scale tests and liquid-phase sorption experiments. The composite sorbents exhibit excellent potential for efficiency enhancement of existing processes by lowering investment and operating costs.

Keywords Gas-phase and liquid-phase sorption · Oxygen VPSA · Mixtures of non-electrolytes · Cu^{2+}-ion kinetics · Zeolites NaX and LiLSX · Zeolite-sorbent shapes · Composites · Sorption-inert cores · Granulation

This paper is dedicated to the memory of John D. Sherman

A. Brandt · B. Unger
Chemiewerk Bad Köstritz GmbH, Heinrichshall,
07586 Bad Köstritz, Germany

M. Bülow (✉)
Am Rökerberg 22, 18347 Ostseebad Dierhagen, Germany
e-mail: martin.bulow@t-online.de

A. Deryło-Marczewska · J. Goworek
Faculty of Chemistry, Maria Curie Skłodowska University,
M. Curie Skłodowska sq. 5, 20-031 Lublin, Poland

J. Schmeißer · W. Schöps
HITK e.V., Michael-Faraday-Str. 1, 07629 Hermsdorf, Germany

1 Introduction

During the past three decades considerable progress has been achieved in cyclic ad-/desorption processes for production of oxygen, O_2, together with remarkable development of related sorbents (MacKee 1964; Chao 1989; Coe et al. 1993; Reiß 1994; Fitch et al. 1995; Kumar 1996). Such pressure-swing adsorption, PSA, and vacuum-pressure-swing adsorption, VPSA, processes are of specific interest from an efficiency point of view for small-to-medium output O_2 generators ($1 \sim 15$ tons p.d. (PSA), $10 \sim 150$ tons p.d. (VPSA) at $90 \sim 93$ (95)% O_2 purity) (Atkinson et al. 1995). In parallel to improvement of technical processes and their engineering, much attention has been paid to the invention, manufacture and utilization of novel types of sorbents including their enhanced interaction properties with nitrogen, N_2, and industrial procedures to create the best-possible shaped materials for those technologies.

In the case of zeolites for sorption-equilibrium processes, the entire volume of sorption-active particles is used, as a rule, since there is no relevant time limitation to the sorption process. A different picture exists in case of fast dynamic sorption processes. If separation of molecules of different types proceeds by rapid swing between ad- and desorption steps, the molecular-transport rate within a sorbent particle may restrict the specific particle-volume faction, which really participates in the process. Usually, only partial utilization of sorption-active phase takes place. The molecular-transport time from the particle's surface into its volume (and back) may limit the possible cycle time, and, in many cases, the efficiency of the entire technical process. Since diffusion of O_2 and N_2 within typical O_2-VPSA zeolite-sorbent crystals is rather fast (Bülow et al. 1996; Bülow and Shen 1998), intraparticle transfer rate of sorbing species may mainly be limited by the "effectiveness" of

the related meso-/macroporous transport system (Bülow and Shen 2004). These considerations lead to the idea of novel material composites for rapid sorption processes that this paper will deal with.

2 Background and formulation of the problem

Technical sorbents and adsorbers for a given process are optimized *inter alia* with respect to their particle shape and size to meet the requirements for sorption, mechanical properties and pressure-drop behavior. In rapid dynamic processes improvement can be achieved, if the time for molecular transfer within a sorbent particle of certain shape is decreased, e.g., by reducing the diffusion-path length or the transport resistance. This can be done by reducing the particle size and/or providing transport pores within the particle to be sufficient in amount and size. Although size reduction of sorbent granules allows for cycle-time reduction that leads to higher productivity per units of volume and time on one and the same amount of sorbent or size of adsorber, this approach is connected with pressure-drop increase and, thus, restricted by a specific particle-size limit.

As well known, in many rapid cycle processes only the outer shell of a given sorbent particle participates in the sorption process while the core remains practically unused during the operation. This suggests a way towards sorbent-performance enhancement, viz., a decrease in the molecular-transport paths can be achieved by using of composite granules comprising a sorption-inert core and a sorption-active shell material (Lü and Bülow 2000; Lü et al. 2001a, 2001b; Monereau et al. 2000; Tang et al. 2001). Identical sorption-kinetic behavior exists for a sorption-active shell/sorption-inert core composite particle and a sorption-active shell/hollow core particle—if their other parameters remain equal (Lü and Bülow 2000). To visualize this approach to materials, an electron micrograph showing a sectional profile of an EPS-polymer-core bead with FAU-zeolite-shell sorbent is shown in Fig. 1. The corresponding hollow bead can be made by thermal removal of the polymeric core.

A performance enhancement by reducing diffusion resistance within sorbent particles of certain shapes requires the existence of transport (meso- and macro) pores therein that have to be sufficient in amount and size. The diameter of said pores should be at least in the range of the mean free path length of the molecules to be ad-/desorbed. Ways were exemplified (Hirano et al. 1990; Brandt et al. 2004) towards appropriate transport pores in FAU-zeolite sorbent particles, which consist of subsequent kneading, shaping and rounding of sorbent bodies. Addition of suitable additives such as fibrous clay (Kawamoto et al. 1999) or thermally degradable spacers (Chao and Pontonio 1999) is possible if the treated

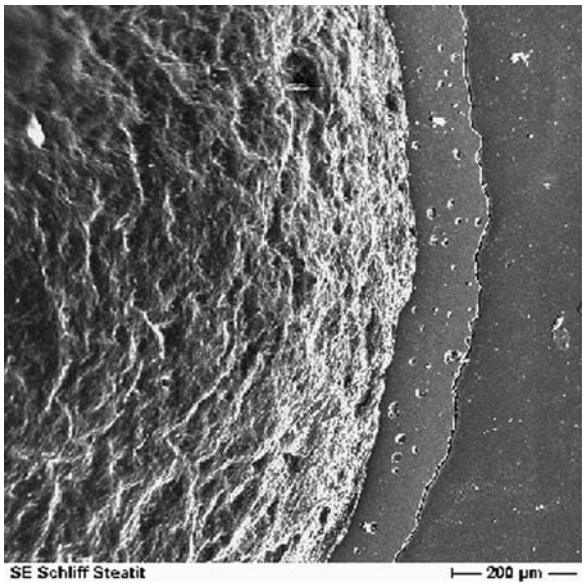

Fig. 1 Sectional profile of a sorption-inert EPS-polymer-core bead covered by sorption-active FAU-zeolite shell to provide a hollow zeolite bead by thermal removal of the organic core

material is resistant with regard to thermal/hydrothermal stress. The "spacing ability" of several selected materials is illustrated by electron micrographs seen in Fig. 2, cf. also Table 1.

Considering the need for secondary pores within a range of at least (200–500) nm, fibrous as well as granule-shaped thermally removable organic materials within the lower µm-size range would meet this requirement, cf. Table 1. A LiLSX zeolite was beaded by using attapulgite clay as binder, and, for comparison, 5 wt-% of two different spacers (either Arbocel BE 600-30 for a short-length cellulose fiber type material, or Cellotin ZZ 8/1 for a long-length cellulose fiber type) were added to the granulation mix. As a result, volume and mean sizes of secondary pores are increased but bulk density is lowered, i.e., a larger porosity with a higher amount of transport pores of the desired size is generated. Different spacers may influence the final bead properties differently, e.g., a longer fiber may cause an even higher porosity with transport pores of larger diameter. Suitable thermally removable spacers allow for tailoring the transport-pore system in sorbent particles.

On the other hand, shaping principles/conditions are specific with regard to the shape type, particular properties of products shaped and their yields. Table 2 gives a summary of commonly used shaping procedures. Having in mind formation of sorption-active shell/sorption-inert core composite granules, suitable plating/coating procedures should be considered, in which a core/seed is used as the base, onto which the sorption-active material is deposited layer by layer. The so-called "rotor-coating" principle often used in the making

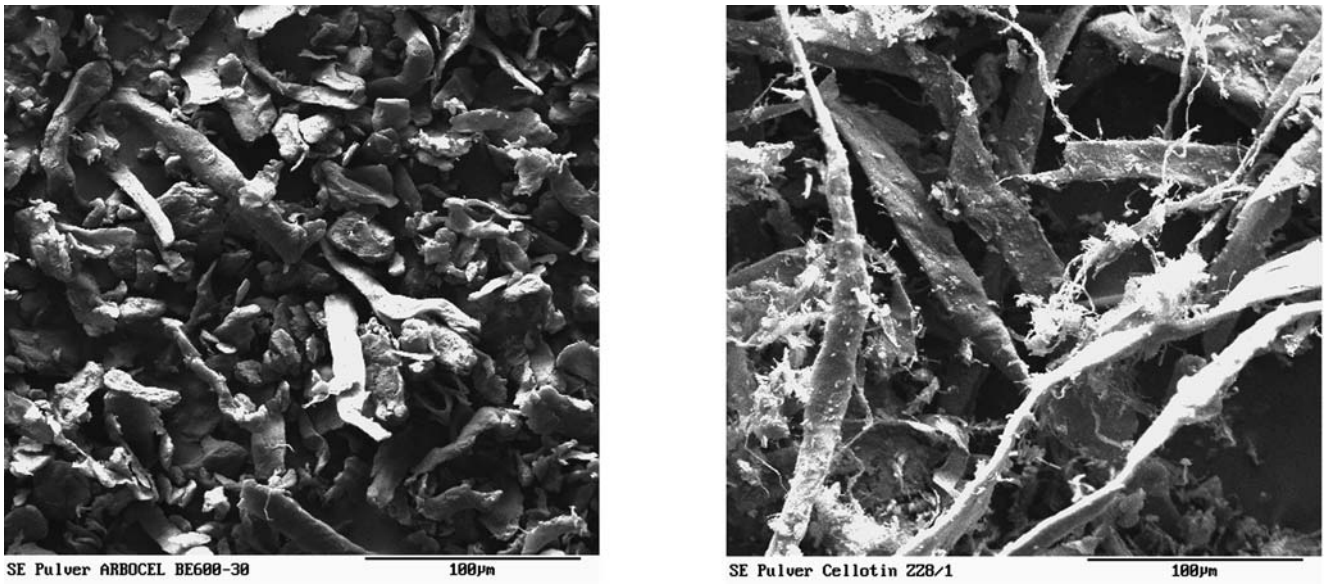

Fig. 2 Structure of thermally removable spacers (Arbocel BE 600-30, *left*; Cellotin ZZ 8/1, *right*) for making sorption-inert core/sorption-active zeolite shell composite materials

Table 1 Transport-pore characteristics generated by using thermally degradable spacers in sorption-active zeolite-shell compounds (LiLSX zeolite/attapulgite clay; 80/20 wt.-%).

No.	Type of spacer	Pore volume[a] ($mm^3\ g^{-1}$)	Mean pore size[a] (nm)	Bulk density[a] ($g\ cm^{-3}$)
1	none	281	120	0.63
2	5 wt.-% Arbocel BE 600-30 *J. Rettenmaier & Söhne*, Germany	374	300	0.56
3	5 wt.-% Cellotin ZZ 8/1 *J. Rettenmaier & Söhne*, Germany	473	330	0.52

[a]Hg high-pressure porosity measurement data

of pharmaceuticals seems to be an interesting embodiment in that respect (Bücheler et al. 1988).

In this paper, the principles for making suitable transport-pore systems in sorption-active zeolite shell/sorption-inert core composites are described, and properties of the latter are specifically discussed with regard to their performance in an O_2-VPSA process. In addition, liquid-phase sorption experiments are presented showing the sorption-kinetic advantages of sorption-active shell/sorption-inert core composites over traditional zeolite-bead materials.

3 Experimental

3.1 Sorbents

All experiments were performed on zeolite-containing beads. Zeolites NaX ($SiO_2/Al_2O_3 = 2.45$) and LiLSX ($SiO_2/Al_2O_3 = 2.01$; $Li^+/\sum$ cations $= 0.96$) were chosen as sorption-active components. An attapulgite clay (CLARSOL ATC-NA—*Atochem*, France; 20.0 wt.-% L.o.I.-corrected content) and a sodium silicate solution ($SiO_2/Na_2O = 3.36$; total solids: 35.9 wt.-%—*Wöllner*, Germany) were used as inorganic binders. Granulation experiments were carried out either by a mixing granulator (*Eirich* R 02) or a laboratory rotor coater (*Glatt* SR 360). All final products were treated in a dry-air-purged pilot calciner under identical conditions, prior to further handling. Structural characterization was done by high-pressure Hg porosimetry (Macropore 120 porosimeter 2000, *Carlo Erba* Instruments). Static N_2-sorption capacity was determined by volumetric technique (Gemini 2370, *micromeritics*).

The zeolite content of the shaped particles was calculated as the ratio between the micropore volumes measured on the beaded material and on the related pure zeolite (NaX or LiLSX). Micropore-volume data required were obtained from N_2-sorption experiments at 77 K and a *t*-plot method using Gemini 2370. Similar zeolite contents of shaped ma-

Table 2 Classification of principles for shaping zeolite-containing sorbents

Basic principle	Granulation method	Granule size[a] (mm)	Yield in straight-run shaping for $d_{max}/d_{min} = 3$	"Sphericity"/r; according to API (1995)	Remarks
Mechanical growth	Disc/pan granulation	0.5–8	30–60	0.7–0.9	Multiple-stage procedure possible
Agglomeration	Drum granulation	0.5–8	40–60	0.7–0.8	Coating possible
Mix granulation	Mix granulation				
	– without high-shear rotating mixing tool	0.6–8	20–60	0.6	
	– with high-shear rotating mixing tool	0.5–6	40–60	0.6–0.7	
Thermally aided granulation	Fluidized-bed granulation	0.1–3	50–80	0.7–0.8	Coating possible by:
	Spray drying	0.01–0.8	70–80	0.9	– top spraying – bottom spraying (acc. to Wurster)
Pressure agglomeration	Extrusion	>1.5	90–100	–	Cylindrical shapes
Coating	Rotor coating	0.5–3	80–90	0.9	High sphericity coating possible

[a]Preferred range, classification based partly on own experience

Table 3 Zeolite-bead samples for liquid-phase sorption-kinetic measurements

Sample code	Granulation method	Core material	Zeolite-bead material[a] (before calcination)	Sieve fraction (mm)
LiLSX (# 02-10-240)	*Eirich* mixer	No inert core	80 wt.-% LiLSX 20 wt.-% attapulgite	2.0–2.36
LiLSX (# 02-07-234)	*Eirich* mixer	Foamed glass (1.18–1.25) mm	80 wt.-% LiLSX 20 wt.-% attapulgite	2.0–2.36

[a]Relevant crystallinity data as well as micro- and mesoporosity properties of these zeolite specimens will be communicated independently

terials were shown to exist from the ratio between static N_2-sorption capacity (25 °C/1000 mbar) of beads and of pure zeolite phase.

Specifically for liquid-phase sorption experiments, two representative samples of LiLSX-zeolite beads were investigated to compare their sorption-kinetic properties, cf. Table 3. Additional experiments were conducted on the basic LiLSX crystallites, from which those bead samples were made. The primary LiLSX crystallites are characterized by nearly a complete cation exchange Li^+ vs. Na^+, cf. above.

3.2 Pilot-scale O_2-VPSA tests

Dynamic sorption-performance data were measured using a pilot-scale O_2-VPSA two-adsorber-bed system (Lü et al. 2004) at 25 °C with VPSA cycles optimized for each zeolite type. For NaX-based particles, the cycle included 8 s each for both ad- and desorption, at a total cycle time (for the two adsorbers) of 30 s, while for LiLSX-based particles the cycle comprised 23 s each for both ad- and desorption, and the total cycle time was 64 s.

3.3 Sorption from solutions—binary non-electrolyte mixtures

In a series of 10 cm^3 screw-capped flasks sealed with Teflon gaskets, c. 1 g of sorbent was mixed with about 4 cm^3 of binary solutions of either (methanol (1) + benzene (2)) or (benzene (1) + n-heptane (2)), in each flask. Due to weak sorbate-zeolite interactions of n-heptane and relatively

strong interaction of methanol and benzene, the two latter components were expected to be preferentially sorbed. Their mole fraction in initial solutions was $x_1^1 \approx 0.3$. The flasks were shaken for a given time in shaker baths thermostatted at 25 °C. The compositions of solutions after different time periods were determined by gas chromatography using a GC *HP* 5890 equipped with a thermal-conductivity detector in hydrogen, H_2, as carrier gas.

In sorption at solid/liquid interface from binary solutions the quantity measured is "surface" excess of component i, $n_i^\sigma = n^0 \Delta x_i^l / mS$, where Δx_i^l is the change in mole fraction of component i when n^0 moles of solution are added to m grams of sorbent with specific "surface" S. For strong preferential sorption, the "surface" excess of component i may be assumed to be the value of its individual sorption, i.e., the real number of moles of component i sorbed per "unit area of the surface" (for microporous materials surface parameters need to be replaced by the corresponding pore volume ones).

3.4 Sorption kinetics of Cu^{2+} ions from aqueous solutions

A series of experimental sets were performed on the bead materials of Table 3. They represent kinetics of cation exchange Li^+ vs. Cu^{2+} (specified by the intraparticle Cu^{2+}-transfer rate) in ammonia, NH_3, used to prevent precipitation due to zeolite-induced pH-value shift. The experiments were executed as follows. A zeolite mass of 2 g was suspended in 64 ml of 0.08 mol/l $Cu(NO_3)_2 \cdot 3H_2O$ (incl. 4 ml NH_3); initial pH = 11.7, to reach a pH ∼ 12 after 3 h. Kinetic curves were built by ca. 90 points each taken after a time interval, 133 s, with a total measurement time of 3 h and 18 min, at 25 °C. A *Cary* 100 UV-VIS spectrophotometer with a flow cell was utilized for analyses, in which the absorption peak of the Cu complexes at 609 nm (wide peak) was used. During experiments the solution was always clear; the absorption peaks did not change either position or shape. The actual sorption experiments were carried out in external *Erlenmeyer* flasks with tightly fitted caps under permanent stirring. Automatic sampling was done by a peristaltic pump (Teflon tubings). After measurement, the solution was returned into the sorption vessel. For the beads, profiles "concentration vs. time" and "sorption vs. time" were calculated from the obtained spectra. For LiLSX *crystallites,* kinetic studies could not be performed, since the flow-cell filter of the UV-VIS spectrophotometer became blocked instantaneously.

To account for the complex character of Cu^{2+}-ion kinetics on zeolites, the multi-exponential equation that corresponds to a series of parallel first-order processes (Ho and McKay 1999) was fitted (Marczewski 2007). The obtained parameters were used for calculation of the sorption curve, $a(t)$:

$$C/C_0 = \sum_{i=1}^{s} A_i \exp(-k_i t) + A_0 \quad \text{where} \quad \sum_{i=1}^{s} A_i = 1 - A_0, \tag{1}$$

$$a(t) = \frac{C_0 V}{m}\left[(1 - A_0) - \sum_{i=1}^{s} A_i \exp(-k_i t)\right]. \tag{2}$$

In the above, C is the actual concentration, C_0 is the initial concentration, m is the sorbent mass, V is the solution volume, t is time, the parameters A denote the total concentration changes, k describes the sorption rate. The value A_0 allows for calculating (extrapolating) concentration C_{eq} and sorption a_{eq}, both at equilibrium.

4 Results and discussion

4.1 Novel composite granules

Based on a theoretical consideration of diffusion in hollow geometries (Lü and Bülow 2000), various technical solutions to the problem of utilizing sorption-active shell/sorption-inert core-composite sorbents have been proposed (Lü and Bülow 2000; Lü et al. 2001a, 2001b; Monereau et al. 2000). Our approach rests on technically relevant issues, viz., if in rapid dynamic ad-/desorption processes—due to fast alternating change between ad- and desorption steps—the sorbent particle is utilized partially only, whereas specifically, the core of such particle does practically not participate in the process at all. Thus, it should be possible to save a major part of the sorption-active material (which nowadays is clearly a higher-added-value and cost-intensive material) by replacing it by a less costly sorption-inert material improving, this way, the overall economics of the entire technical process. In addition, it should become possible to control the overall bulk density of the sorbent composite by selecting an appropriate core material without influence on the density of the sorption-active shell. The latter feature could be advantageous if, for example, higher gas velocities through an adsorber bed were required, but were not feasible traditionally due to bed-fluidization behavior. A high-density core material could provide sorbent particles with higher bulk density and, thus, higher bed-fluidization resistance.

Common-composition zeolite-binder mixtures that are based on zeolites NaX and LiLSX were deposited on various core materials, cf. Tables 4 and 5. A wide range of potential core materials was considered in terms of density and porosity, from low-density foamed-glass beads and inert low-cost zeolite beads to high-density quartz-sand grains.

Deposition/coating was carried out by an *Eirich*-type mixing granulator and a *Glatt*-type rotor coater. Despite difficulties in getting reliable profile pictures of composite beads, Fig. 3 allows for some insight into the cross profiles of foamed-glass-core zeolite LiLSX composite beads (left) and quartz-sand-core zeolite LiLSX composite beads (right). In the former case, one can clearly distinguish between regular structures of both the foam core and the dense sorption-active shell. In the latter case, quartz cores yield irregular shapes with uneven thickness of the zeolite-binder coat, cf. below.

4.2 O_2-VPSA test results

Relevant material properties and O_2-VPSA performance results of sorption-active NaX shell/sorption-inert core-composite sorbent granules are given in Table 4 in comparison with a state-of-the-art "full-body" NaX zeolite sample, # 1. The latter one is beads, (1.6–2.5) mm (approx. 8 × 12 mesh) in size, as used usually for PPU up-front cryogenic air-separation units and, occasionally, in O_2-VPSA plants as well. Samples # 2–4 were made of foamed-glass beads as core material of identical size, (1.18–1.25) mm, but with different final product bead sizes.

The zeolite content (column 6) as determined by independent methods decreases with decreasing size of final beads. Such dependence is also found for bulk density (column 5) with a much lower bulk density of foamed-glass-based beads as compared to the "full- body" zeolite material. Both dependences are caused by a decrease in core/coating material ratio with increasing final-bead size, i.e., with decreasing thickness of the sorption-active shell. A similar sequence holds for the volume-related productivity in pilot-plant O_2-VPSA tests, both at 90% (column 7) and at 93% (column 10) O_2 purity. Since a given bed volume contains a lower amount of sorption-active material as compared to # 1, the volume-related productivity should also decrease. The dependence of productivity on zeolite content of the related bead fraction (columns 8 and 11) is more interesting. First, said productivity is higher than the productivity values found for "full-body" beads in all monitored cases, i.e., utilization of the zeolite constituent in the coated material exceeds that of the "full-body" zeolite material at given bead size in all cases. The zeolite-related productivity of samples # 2–4 exhibits a maximum at bead size, (1.7–2.0) mm, of final product. This feature, unexpected at first glance, could be due to the existence of an *optimum* value in the thickness of the sorption-active compound shell. Increasing the shell thickness leads first to an increase in zeolite-content related productivity, but if a certain *optimum* thickness is exceeded, this productivity may tend towards the "full-body" material value. As expected by implying shorter diffusion pathways, the yield of produced O_2 becomes less sensitive to product purity.

Samples # 5 and 6 are prepared as samples # 2–4 but using a rotor coater instead of the *Eirich* mixer. There is no significant difference in the properties of final sorption-active shell/sorption-inert core composite beads between the two methods for a given system.

In samples # 7 and 8, low-cost NaA-zeolite-containing beads were used as core material. To avoid any secondary effect by this core material on sorption behavior, the core material was pre-calcined at different temperatures, 700 and 1000 °C. The sizes of the final composite beads are identical. The zeolite contents and bulk densities for products made of core material calcined at higher temperature were found to be higher. Calcination at 1000 °C leads obviously to an increase in bead-core density accompanied by bead shrinkage confirmed independently. If the size of final (coated) beads is the same in both cases, (1.7–3.15) mm, the average thickness of sorption-active material layer should be larger in case of core beads pre-calcined at 1000 °C. In this respect, all findings on samples # 7 and 8 can be explained as before, viz., lower shell thickness causes lower volume-related O_2 enrichment, the zeolite-amount-related productivity increases as well (increasing thickness of the sorption-active shell leads still to performance increase). A relatively low yield obtained by the O_2-VPSA test for this sample and its strong decrease with increasing O_2 purity could be explained by a somewhat incomplete inertization of the NaA-zeolite core during calcination at 1000 °C.

Samples # 9 to 11 are materials based on quartz-sand granules as sorption-inert cores. The bulk density of quartz is highest in the row looked at. Comparably low zeolite content in the adsorber bed ought to be considered from this point of view. Since zeolite content is always related to the mass of the entire final bead product, a heavier core material would always lead to a lower content of shell material, although the volume of the shell may be same. If one compares sample # 10 (based on quartz sand, (1.18–1.25) mm) with a final bead product of size, (1.7–2.36) mm, with final samples # 3 and 6 that have foamed-glass cores at the same geometric relations, the volume-related productivities at 90% and 93% O_2 purity turn out to be nearly the same for all samples under question, which would support the aforementioned assumption. Slightly higher numbers for quartz-sand-bead based materials could be due to irregularly shaped cores as mentioned above, which are connected with uneven thicknesses of sorption-active material shells, i.e., a higher volume-related content of sorption-active material. The higher yield of quartz-based particles compared to foamed-glass based ones may also be due to full inertness of the quartz cores in opposite to foamed-glass bodies, in which certain diffusion capabilities may exist.

Table 5 presents results for composite granules with LiLSX zeolite as sorption-active component. Commercial "full-body" LiLSX beads, (1.6–2.5) mm, are used as reference material. Qualitatively, the results correspond to those

Table 4 Description of composite-granule samples and results of O_2-VPSA pilot-plant experiments at 25 °C (composition of sorption-active component: NaX zeolite/attapulgite clay, 80/20 wt.-%)

1	2	3	4	5	6	7	8	9	10	11	12
No.	Core material	Coating device	Composite granule size (mm)	Bulk density (VPSA device) (g/l)	Zeolite content (wt.-%)	Volume-related productivity ($I_N O_2\ l^{-1}\ h^{-1}$ at purity 90% O_2)	Zeolite-content-related productivity[a] ($I_N O_2\ kg_{zeo}^{-1} h^{-1}$ at purity 90% O_2)	Yield (% at purity 90% O_2)	Volume-related productivity ($I_N O_2\ l^{-1}\ h^{-1}$ at purity 93% O_2)	Zeolite-content-related productivity[a] ($I_N O_2\ kg_{zeo}^{-1}$ at purity 93% O_2)	Yield (% at purity 93% O_2)
1 (cf. Reiß 1994)	Standard granules (no sorption-inert core)	–	1.6–2.5	700	83	46.6	80.2	43	41.4	71.3	40
2	Foamed-glass granules, 1.18–1.25 mm	*Eirich* mixing granulator, R02	2.0–2.36	553	72	40.3	101.1	43	37.5	94.3	42
3	Foamed-glass granules, 1.18–1.25 mm	*Eirich* mixing granulator, R02	1.7–2.0	506	64	36.0	111.2	43	34.6	106.9	43
4	Foamed–glass granules, 1.18–1.25 mm	*Eirich* mixing granulator, R02	1.4–1.7	419	59	23.3	94.2	37	22.2	89.8	36
5	Foamed-glass granules, 1.18–1.25 mm	*Glatt* rotor coater, SR 360	2.0–2.36	541	72	40.2	103.2	45	37.3	95.8	43
6	Foamed-glass granules, 1.18–1.25 mm	*Glatt* rotor coater, SR 360	1.7–2.0	515	64	37.1	112.7	44	35.4	107.5	44
7	Type A zeolite-containing beads calcined at 700 °C, 1.4–2.0 mm	*Eirich* mixing granulator, R02	1.7–3.15	756	35	26.8	101.1	35	20.7	78.3	28
8	Type A zeolite-containing beads calcined at 1000 °C, 1.4–2.0 mm	*Eirich* mixing granulator, R02	1.7–3.15	896	42	39.6	105.2	47	37.2	98.8	46
9	Quartz sand, 1–2 mm	*Glatt* rotor coater, SR 360	1.6–2.8	976	44	42.0	97.7	46	38.4	89.3	44
10	Quartz sand, 1.18–1.25 mm	*Glatt* rotor coater, SR 360	1.7–2.36	981	36	39.1	110.8	46	37.5	106.1	46
11	Quartz sand, 1.0–1.5 mm	*Glatt* rotor coater, SR 360	2.0–2.8	904	46	44.2	106.3	48	40.9	98.5	46

[a]Mass-related productivity divided by zeolite content as given in column 6

Table 5 Description of composite-granule samples and results of O_2-VPSA pilot-plant experiments at 25 °C (composition of sorption-active component: LiLSX zeolite/attapulgite clay, 80/20 wt.-%)

1	2	3	4	5	6	7	8	9	10	11	12
No.	Core material	Coating device	Composite granule size (mm)	Bulk density (VPSA device) (g/l)	Zeolite content (wt.-%)	Volume-related productivity ($I_N O_2\ l^{-1}\ h^{-1}$ at purity 90% O_2)	Zeolite-content-related productivity[a] ($I_N O_2\ kg_{zeo}^{-1}\ h^{-1}$ at purity 90% O_2)	Yield (% at purity 90% O_2)	Volume-related productivity ($I_N O_2\ l^{-1}\ h^{-1}$ at purity 93% O_2)	Zeolite-content-related productivity[a] ($I_N O_2\ kg_{zeo}^{-1}$ at purity 93% O_2)	Yield (% at purity 93% O_2)
12 (Ref. [2])	Standard granules	–	1.6–2.5	700	83	58.1	100.0	65	52.5	90.4	62
13	Foamed-glass granules, 1.0–1.5 mm	*Glatt* rotor coater, SR 360	2.0–2.8	511	76	44.6	114.7	64	41.9	107.8	63
14	Quartz sand, 1.0–1.5 mm	*Glatt* rotor coater, SR 360	2.0–2.8	910	40	50.6	139.0	67	47	129.2	66
15	Quartz sand, 1.18–1.25 mm	*Glatt* rotor coater, SR 360	2.0–2.8	820	54	52.5	118.7	67	47.6	107.6	65
16	Quartz sand, 1.25–1.5 mm	*Glatt* rotor coater, SR 360	2.0–2.8	893	40	54.1	151.5	70	50.6	126.5	69

[a]Mass-related productivity divided by zeolite content as given in column 6

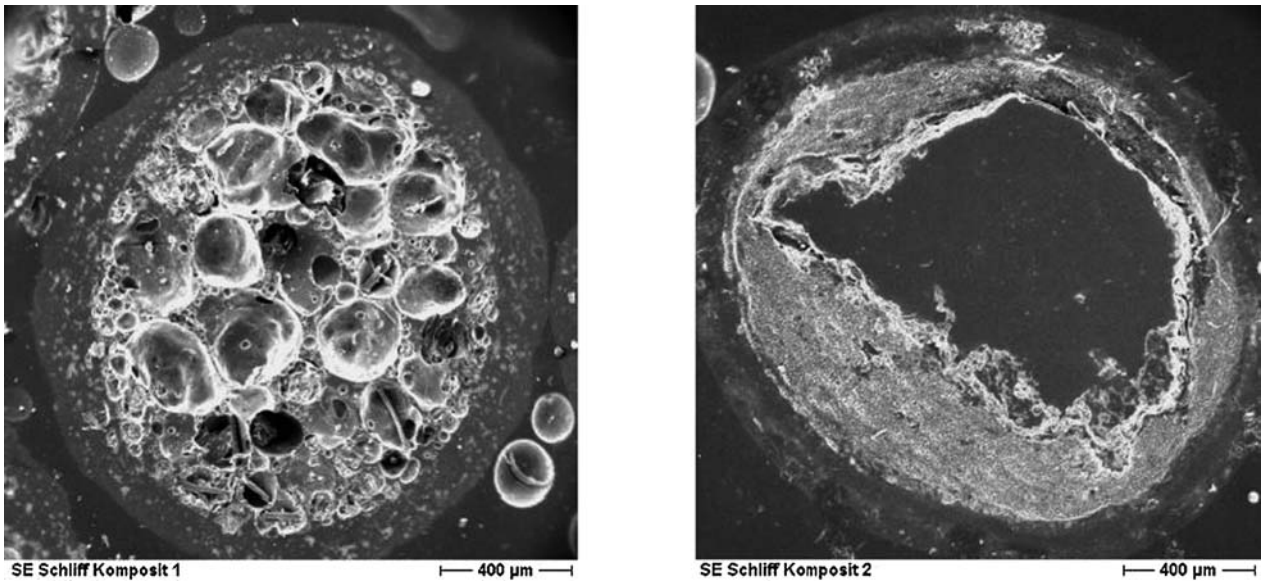

Fig. 3 Sorption-active shell/sorption-inert core zeolite LiLSX-composite granules with core materials foamed-glass granules (*left*) and quartz-sand grains (*right*)

obtained for the NaX-zeolite containing materials. In all cases, a higher zeolite-content-related O_2-VPSA performance is found in comparison to that of the commercial "full-body" material, i.e., the LiLSX-based composite material exhibits a higher utilization of the zeolite component.

Comparing the behaviors of samples # 13 (foamed-glass core) and # 14 (quartz-sand core) prepared under identical conditions and in equal particle geometries, a higher bulk density and a lower mass-related zeolite content is found for the quartz-sand-containing material. On the other hand, a remarkably higher volume-related O_2-VPSA performance is found for the quartz-sand-based composite in both O_2 purity regions. The zeolite-content-related productivity of the quartz-sand-containing beads strongly exceeds that of the foamed-glass-containing beads due to better utilization of the zeolite component. Consequently, considering the same sorption-active component volume in samples # 13 and 14 with identical geometry, the volume-related productivity has to be lower in case of the lower utilization of the zeolite component. If samples # 14 and 16 are compared with each other, which all consist of quartz-sand-core material of differing size, (1.0–1.5) mm, (0.8–1.25) mm, and (1.25–1.5) mm, but are coated to yield the same final bead size, (2.0–2.8 mm), one finds a clear bulk-density sequence that corresponds to the size of the core beads used: the smaller the core beads, the lower the bulk density.

The zeolite content as measured by independent methods shows its highest value in the case of the smallest core beads, but no difference seems to exist between core beads of (1.0–1.5) mm and (1.25–1.5) mm. The difference in the amounts of "on-coated" material does not differ much in these cases. This assumption is supported by the small deviation in their bulk densities. Consequently, considering the same sorption-active component volume in samples # 13 and 14 with identical geometry, the volume-related productivity has to be lower in case of the lower utilization of the zeolite component. If samples # 14 and 16 consisting of quartz-sand-core material of differing size (1.0–1.5 mm, 0.8–1.25 mm and 1.25–1.5 mm) but coated to yield the same final bead size, (2.0–2.8 mm), are compared, one finds a clear bulk-density sequence that corresponds to the size of the core beads used: the smaller the core beads, the lower the bulk density. The zeolite content as measured by independent methods shows its highest value in case of the smallest core beads, but no difference seems to exist between core beads of (1.0–1.5) mm and (1.25–1.5) mm. The difference in the amounts of "on-coated" material does not vary much in these cases. This assumption is supported by only a slight deviation in their bulk densities.

At first surprisingly, the volume-related productivity of samples # 14 to 16 does not follow the expected sequence, i.e., the smaller the sorption-inert core, the larger the volume of the sorption-active shell, and, thus, the larger the volume-related productivity. In the given case, however, the sequence of increasing volume-related productivity should be as follows: # 16 followed by # 14, followed by # 15. Obviously, this is a situation similar to that described before: utilization of the zeolite component (cf. zeolite-content-related productivities) exhibits its lowest value for # 15 (with the thickest sorption-active shell), followed by # 14, which should be situated in the middle, from the shell-thickness point of view. But as seen already, there is, obviously, no big difference in shell thickness between samples # 14 and 16. Therefore, zeolite utilization seems to play the dominant

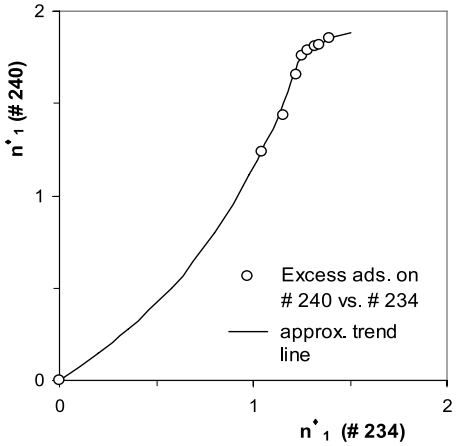

Fig. 4 Ratio of excess sorption values for liquid mixtures (benzene (1) + n-heptane (2)) on beaded LiLSX samples # 234 and # 240 of Table 3

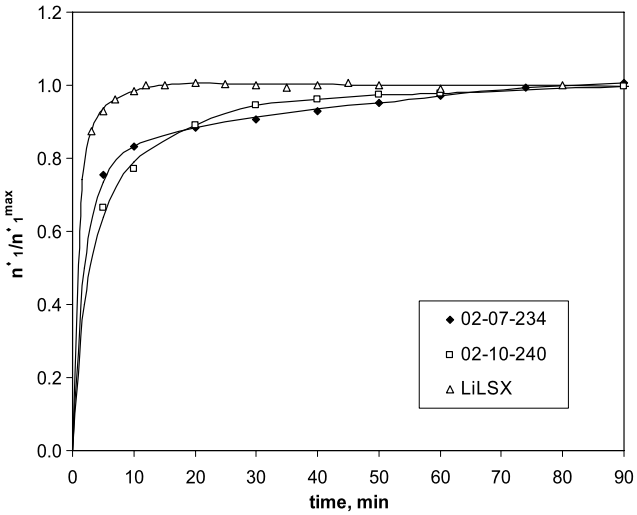

Fig. 5 Relative excess sorption $n_1^{\sigma}(t)/n_1^{\sigma\,\max}$ of benzene (1) from n-heptane (2) solutions for samples of Table 3. LiLSX denotes the crystalline material

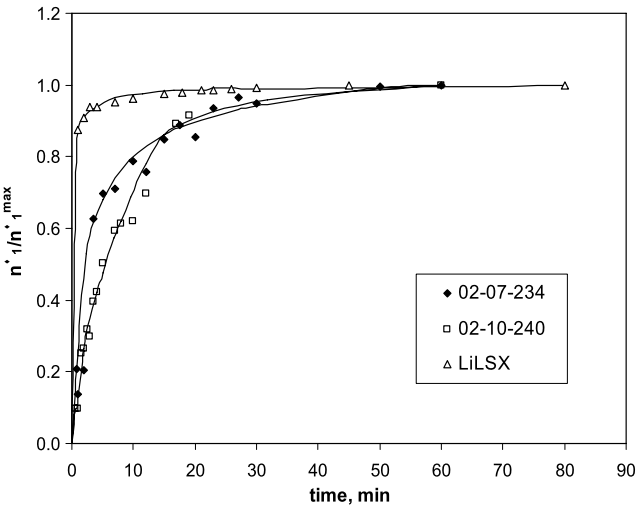

Fig. 6 Relative excess sorption $n_1^{\sigma}(t)/n_1^{\sigma\,\max}$ of methanol (1) from benzene (2) solutions for samples of Table 3. LiLSX denotes the crystalline material

role, i.e., # 16 shows a higher volume-related productivity than # 14. Although close, # 16 does not reach the volume-related productivity measured on the reference material. A comparison of the zeolite contents per sorbent volumes ("zeolite density" as product of bulk density, column 5, and zeolite content, column 6) shows that at a "zeolite density" of 61% in case of sample # 16 related to the reference sample, the volume-related productivity is lower by only 6.9% at 90% O_2 purity, and by 3.6% at 93% O_2 purity. A slight increase in sorbent volume would lead to the same performance in O_2 VPSA, but *at much lower zeolite content in the sorbent*. As in the case of the NaX-zeolite-shell component, quartz-sand-based particles provide a higher overall O_2 yield than the classical beads as well as the foamed-glass-based composite particles. At the same time, the yield of O_2 produced remains nearly unchanged with increasing O_2 purity. This may be a direct result of optimized diffusion pathways, which allows for high sorption selectivity for N_2 over O_2 under dynamic conditions. In addition, a shorter desorption time is required for achieving the same residual vacuum by using the same vacuum-pump sizes and energy consumption. The significant increase in yield is an important factor for the practical applicability of the general idea (Lü and Bülow 2000) developed specifically towards materials that ensure decrease in investment and operating costs in rapid sorption-separation processes such as O_2 VPSA.

4.3 Liquid-phase sorption kinetics of binary mixtures

The results for liquid mixtures (benzene + n-heptane) and (methanol + benzene) on beaded LiLSX zeolite samples # 234 and # 240 as well as on LiLSX crystallites as presented in Figs. 4–6, demonstrate two effects: (i) uptake of the preferentially sorbed component is governed mainly by zeolite-sorbate interactions, and (ii) comparison of sorption rates in the small-time region shows characteristic differences between the two LiLSX-zeolite sorbent beads # 240 (without sorption-inert cores) and # 234 (with sorption-inert foamed-glass cores). The second effect that depends on kinetic properties of the systems is well visualized if sorption is expressed as a relative quantity, i.e., sorption at given time t to maximum sorption at equilibrium (plateau value in plots of kinetic curves), $n_1^{\sigma}(t)/n_1^{\sigma\,\max}$. Quantification by a curve-fitting procedure is not satisfactory for the non-electrolytes mixtures due to few experimental kinetic points for the samples investigated. But as shown in Fig. 4 that expresses the ratio of sorption values in the binary system (benzene + n-heptane) for the two LiLSX-bead types of Table 3, sorption in the small-time region is quicker for the sample # 234 (with sorption-inert cores) than for the sample # 240 (without inert cores). Sorption-kinetic curves for methanol from

benzene solutions and benzene from n-heptane solutions on zeolite-bead samples # 240 (without sorption-inert cores) and # 234 (with sorption-inert foamed-glass cores) are presented in Figs. 5 and 6.

For these two systems, the bead sample with sorption-inert cores, # 234, compared to those without such cores, shows higher sorption rate in the small-time region ($t <$ 10 min).

In the case of the original crystalline unshaped LiLSX material, the sorption-uptake rate of the preferentially sorbing species is observed to be fastest for both binary liquid systems. This result for the parent zeolite crystals may probably be related to their different apparent surface properties compared to those of the beaded samples, which contain attapulgite as binding agent and a significant mesoporosity in addition. The latter conclusion could be supported independently by *Fourier*-transform Infra-red photo-acoustic spectra measured for the three samples (Goworek and Bülow 2005) and pore-size distribution curves based on measurement of argon, Ar, ad-/desorption isotherms measured at liquid-Ar temperature and evaluated by a non-local density functional theory (NLDFT) method (Ravikovich and Bülow 2005).

4.4 Sorption kinetics of Cu^{2+} ions from aqueous solutions

Sorption-kinetic (cation-exchange-kinetic) curves for Cu^{2+}-ions from aqueous solutions obtained for the two LiLSX-bead types # 240 (without sorption-inert cores) and # 234 (with sorption-inert foamed-glass cores) are presented in Fig. 7 as dependences of "concentration vs. time", $C = f(t)$, and "sorption vs. time", $Ads = a(t) = f(t)$. Generally, kinetics are found to be quicker on sample # 234 that contains sorption-inert cores. A stronger decrease of concentration is observed at the start of experiment followed by an exponential decrease which is characteristic of pseudo-first-order kinetics (Ho and McKay 1999). The solid lines in Fig. 7 represent the theoretical profiles C vs. t and Ads vs. t calculated by fitting (1). Good agreement between the experimental points and the theoretical curves confirms the choice of a multi-exponential equation to describe sorption kinetics of Cu^{2+} ions on the zeolites studied. For comparison, a typical *Lagergren* plot (Lagergren 1898) is presented in Fig. 8 (sorption equilibrium values were calculated using A_0 from Table 5). It becomes obvious that the process cannot be described by such a simple pseudo-first-order dependence.

The values of the parameters of (1) obtained by curve fitting are shown in Table 6. A_0 is bigger for # 240, which corresponds to a smaller equilibrium sorption (extrapolated) on this sample compared to that on # 234.

The other parameters are divided into three groups: fast-, medium- and slow-stage parameters. The fast-stage parameters describe the initial stronger decrease of concentration; however, the slow-stage corresponds to concentrations close to the equilibrium value. Comparing the total amounts sorbed in the fast and medium processes (A_1, A_2), one can see that they are higher for sample # 234 confirming the quicker kinetics for this material. However, the A_3 parameter is lower for sample # 234 in comparison to that of # 240 because the last, slow stage of sorption process corresponds to equilibrium, which was practically established in the system "Cu^{2+}-ion/zeolite sample # 234".

The parameter A_3 is much larger for the material sample # 240, because for the sample # 234 equilibrium was already practically attained. The ratio of (fast + medium)/slow A parameters is much higher for sample # 234, which means that the sorption process is faster for this system, especially in the first and medium stages. The ratio fast/(medium + slow) is also higher for the sample # 234; however, this difference is smaller.

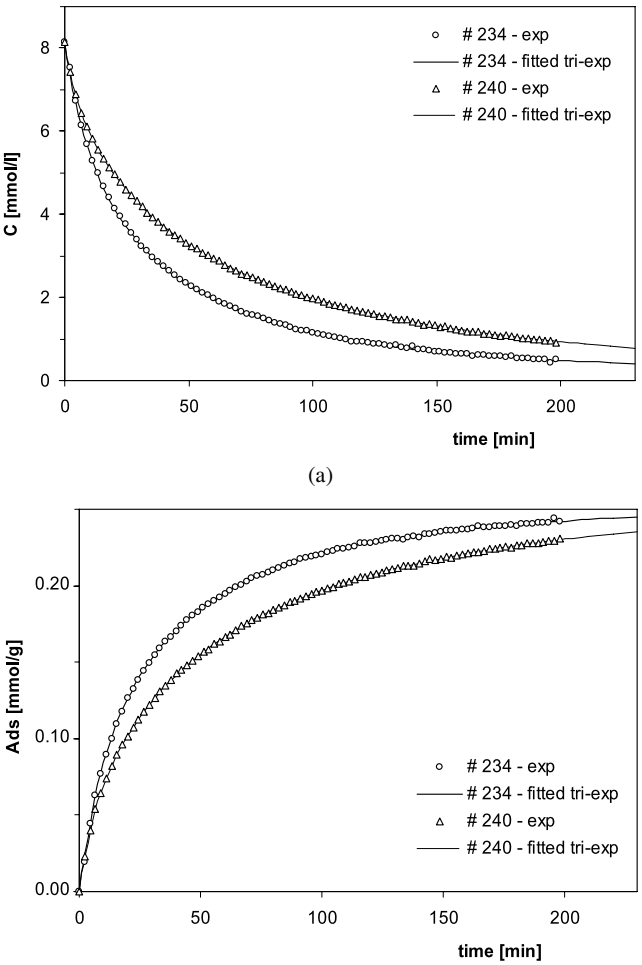

Fig. 7 Concentration (**a**) and sorption (**b**) vs. time profiles for Cu^{2+}-ion sorption from aqueous phase on two beaded zeolite samples, cf. Table 3 (*curves* represent fitted lines with the parameters of (1) as listed in Table 6)

Table 6 Fitted parameters for multi-exponential kinetic curves, (1)

Sample	Fast stage		Medium stage		Slow stage		Equil.	(Fast + medium)/slow	Fast/(medium + slow)
	A_1	k_1	A_2	k_2	A_3	k_3	A_0	$(A_1 + A_2)/A_3$	$A_1/(A_2 + A_3)$
# 234	0.295	0.111	0.509	0.026	0.186	0.0070	0.0100	4.3	0.43
# 240	0.141	0.202	0.294	0.039	0.524	0.0100	0.0406	0.83	0.17

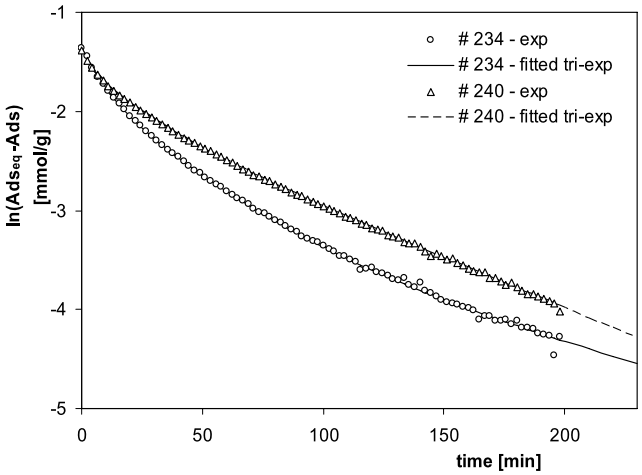

Fig. 8 *Lagergren* pseudo-first-order plot for Cu^{2+}-ion sorption from aqueous phase on two beaded zeolite samples, cf. Table 3 (*curves* represent fitted lines with the parameters of (1) as listed in Table 6)

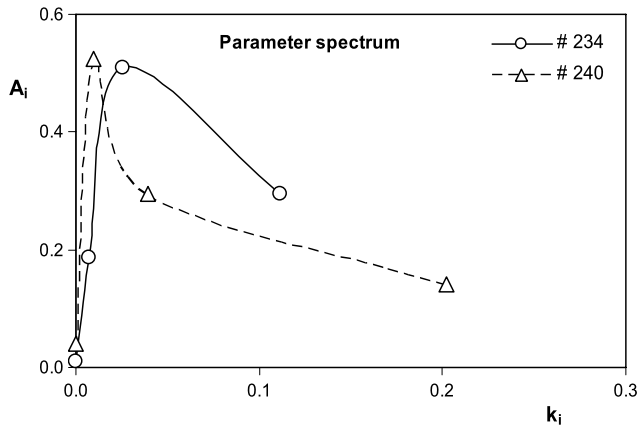

Fig. 9 Comparison of kinetic *parameter spectra* for material samples # 234 and # 240

Unexpectedly, the values of corresponding kinetic parameters k are lower for sorption on sample # 234 compared to that on sample # 240 (cf. Table 6). Such a tendency may be a result of the very beginning stage of sorption ($t < 4$ min) when the process is more rapid on sample # 240, possibly because of either different amounts of dust therein or some variation of conditions that are difficult to control before the system became stable (stirring, etc.). However, if we compare the entire sets of values of fitted parameters A_i and k_i

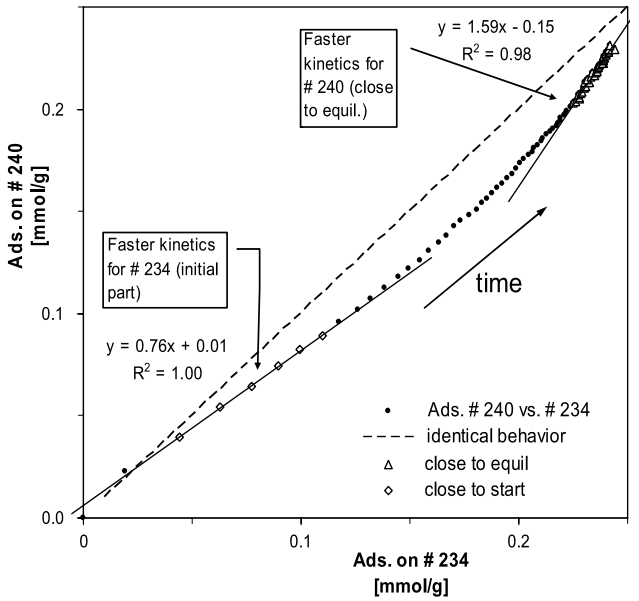

Fig. 10 Comparison of sorption of Cu^{2+} ions between zeolites # 240 (beads without sorption-inert cores) and # 234 (beads with sorption-inert cores)

(see Fig. 9)—here they are called *parameter spectra*—it becomes quite obvious that, in general, the kinetics on sample # 234, i.e., with sorption-inert cores, are faster compared to those on sample # 240, i.e., without sorption-inert cores (shift towards higher kinetic coefficients).

The differences in kinetics of Cu^{2+}-ion sorption on both bead types of LiLSX zeolite may be usefully compared as the dependence of sorption on the sample # 240 vs. sorption on sample # 234 (Fig. 10). Three stages are observed on the experimental dependence. For the initial stage, faster kinetics is found for the system "sample # 234—Cu^{2+} ion". In the medium stage the kinetics becomes comparable for the two types of zeolite beads. Closer to the sorption-equilibrium stage, the process becomes quicker for sample # 240. However, in general, the entire process proceeds more rapidly on the material sample # 234, i.e., on zeolite-sorbent beads with sorption-inert cores.

5 Conclusions

Novel zeolite-composite granules technology based on theoretical consideration of diffusion in hollow geometries sat-

isfy the demand for sorbents for rapid sorption-dynamic processes. Relevant features are higher flexibility in sorbent tailoring to specific processes, excellent sorption properties and increased performance vs. cost ratio. Known coating methods such as mix granulation and rotor coating can be used to make sorption-inert-core containing sorbent beads covered by sorption-active zeolite shells. Foamed-glass beads, inertized zeolite-containing beads and quartz-sand grains were tested successfully as sorption-inert core materials. Using these core materials, final bead materials with a rather wide overall bulk-density range can be provided. For all cases investigated, the O_2-VPSA-process performance utilizing the novel zeolite-bead compounds exceeded that of the processes with corresponding commercial "full-body" zeolite-sorbent materials, specifically at much lower sorbent-volume-related zeolite content. Using density variation of sorption-inert core materials allow for tailoring sorbents to specific process modifications, e.g., for horizontal or vertical O_2-VPSA-adsorber beds, to increase utilization of the sorption-active phase and to optimize overall bead size, sorbent-bulk density, secondary-pore-related mass transfer, bed-pressure drop, and gas flow. This approach makes it possible to avoid bed fluidization without "full-body" material densification by introducing mechanical energy during granulation. Since the sorbent represents a major part of the investment for an entire VPSA plant, its cost reduction would improve the economic efficiency of the entire process.

The findings for the gas-phase O_2-VPSA pilot-plant process were complemented by results of lab-scale investigations of liquid-phase sorption processes, in particular, in systems liquid non-electrolyte mixtures, (benzene + n-heptane) and (methanol + benzene), and sorption kinetics of Cu^{2+} ions from aqueous solutions on beaded LiLSX zeolite materials with and without sorption-inert cores. In all cases apparent sorption kinetics on materials with sorption-inert cores was shown to proceed more rapidly. Thus, the original theoretical concept of zeolite-composite beads with sorption-inert cores is confirmed in practice for rapid gas- and liquid-phase sorption processes.

Acknowledgements The authors are grateful to the *Federal Department of Economy and Labor* of Germany for financial support (chapter 0902, title 685 54, project registration no. 311/01). They also thank the former *The BOC Group* for financial support and fruitful collaboration.

References

API (American Petroleum Institute): Recommended Practices for Testing High-Strength Propants Used in Hydraulic Fracturing Operations, RP 60 (1995)

Atkinson, T., Bülow, M., Fitch, F.R., Doong, Sh.-J., Hirooka, E., Ambriano, J., Petras, R.: Advances in VSA technology for on-site oxygen production. BOC Technol. (2), 29–36 (1995)

Brandt, A., Lübke, M., Schmeißer, J., Schöps, W., Tschritter, H., Unger, B.: Ceramic absorption-desorption body for dynamic separation of two gases as used in pressure- and temperature-change absorption process. DE Patent Appl. 102 13 922 (2004)

Bücheler, M., Schmoll, J., Metzger, K.-L., Luchtenberg, H.: Verfahren zur kontinuierlichen Herstellung von sphärischen Granulaten. DE Patent 36 23 321 A1 (1988)

Bülow, M., Shen, D.: Transport properties of oxygen and nitrogen in CaA-type zeolites. In: Rozwadowski, M. (ed.) Proc. 3nd Polish-German Zeolite Colloquium, pp. 285–294. Nicholas Copernicus University Press, Torun (1998)

Bülow, M., Shen, D.: Mobility of nitrogen in Li,RE-LSX zeolite beads. Stud. Surf. Sci. Catal. **154B**, 2070–2077 (2004)

Bülow, M., Micke, A., Murray, J.W.: Molecular mobility of oxygen in CaA-type zeolite. In: LeVan, M.D., Knaebel, K.S. (eds.) Proc. 5th Int. Conf. Fundam. of Adsorption, pp. 139–147. Kluwer, Norwell (1996)

Chao, C.-C.: Process for separating nitrogen from mixtures thereof with less polar substances. US Pat. 4,859,217 (1989)

Chao, C.-C., Pontonio, S.: Advanced adsorbent for PSA. WO Pat. 99/43415 (1999)

Coe, C.G., Kirner, J.F., Pierantozzi, R., White, T.R.: Nitrogen adsorption with a divalent cation exchanged lithium X-zeolite. US Pat. 5,258,058 (1993)

Fitch, F.R., Bülow, M., Ojo, A.F.: Adsorptive separation of nitrogen from other gases. US Pat. 5,464,467 (1995)

Goworek, J., Bülow, M.: Unpublished results (2005)

Hirano, Sh., Kawamoto, T., Nishimura, T., Yoshimura, K.: Adsorbent for separating gases. Europ. Pat. 0 940 174 A2 (1990)

Ho, Y.S., McKay, G.: The sorption of lead (II) ions on peat. Water Res. **33**, 578–584 (1999)

Kawamoto, T., Nishimura, T., Yoshimura, T.: X-Zeolite bead compact and its production. Jap. Pat. 11 2 46 282 (1999)

Kumar, R.: Vacuum swing adsorption process for oxygen production—a historical perspective. Sep. Sci. Technol. **31**, 877–893 (1996)

Lagergren, S.: Zur Theorie der sogenannten Adsorption gelöster Stoffe. Kungl. Svenska Vettenskapsakad. Handl. **24**, 1–39 (1898)

Lü, Y., Bülow, M.: Analysis of diffusion in hollow geometries. Adsorption **6**, 125–136 (2000)

Lü, Y., Bülow, M., Shen, D., Acharya, D., Andrecovich, M.J., Fitch, F.R., Ojo, A.F.: Composite adsorbent beads for the pressure swing adsorption processes. US Pat. 6,284,021 B1 (2001a)

Lü, Y., Bülow, M., Doong, Sh.-J., Shen, D., Acharya, D., Andrecovich, M.J., Fitch, F.R., Ojo, A.F.: Gas separation process using composite or hollow adsorbent beads particles. Europ. Pat. 1 080 771 A1 (2001b)

Lü, Y., Doong, Sh.-J., Bülow, M.: Pressure-swing adsorption using layered adsorbent beds with different adsorption properties:—experimental investigation. Adsorption **10**, 267–275 (2004)

MacKee, D.W.: Separation of oxygen-containing mixture. US Pat. 3,140,933 (1964)

Marczewski, A.W.: Kinetics and equilibrium of adsorption of organic solutes on mesoporous carbons. Appl. Surf. Sci. **253**, 5818–5826 (2007)

Monereau, Ch., Moreau, S., Ming, S.L.: Utilization d'un adsorbant particulaire non-homogene dans un procede de separation de gaz. French Pat. 2,794,993 A1 (2000)

Ravikovich, P.I., Bülow, M.: Unpublished results (2005)

Reiß, G.: Status and development of oxygen generation processes on molecular sieve zeolites. Gas Sep. Purif. **8**, 95–99 (1994)

Tang, Y., Wang, Y.-J., Wang, X.-D., Yang, W.-L., Gao, Z.: Fabrication of hollow fibers and spheres composed of zeolites by layer-by-layer adsorption method. In: Galarneau, A., Di Renzo, F., Fajula, F., Vedrine, J. (eds.) Zeolites and Mesoporous Materials at the Dawn of the 21st Century: Proceedings of the 13th International Zeolite Conference, Montpellier, France, 8–13 July 2001. Studies in Surface Science and Catalysis, vol. 135. Elsevier, Amsterdam (2001) Compact disc version: Paper no. 21-P-06